

Patterns of Gravitational Cooling in Schrödinger Newton System

DONGSU BAK,^{a,c} SEULGI KIM,^{a,c} HYUNSOO MIN,^a JEONG-PIL SONG^b

a) Physics Department, University of Seoul, Seoul 02504 KOREA

b) Department of Chemistry, Brown University, Providence, RI 02912 USA

c) Natural Science Research Institute, University of Seoul, Seoul 02504 KOREA
(dsbak, hsmi@uos.ac.kr, seulgi.kim@cern.ch, jeong_pil_song@brown.edu)

ABSTRACT

We study time evolution of Schrödinger-Newton system using the self-consistent Crank-Nicolson method to understand the dynamical characteristics of nonlinear systems. Compactifying the radial coordinate by a new one, which brings the spatial infinity to a finite value, we are able to impose the boundary condition at infinity allowing for a numerically exact treatment of the Schrödinger-Newton equation. We study patterns of gravitational cooling starting from exponentially localized initial states. When the gravitational attraction is strong enough, we find that a small-sized oscillatory solitonic core is forming quickly, which is surrounded by a growing number of temporary halo states. In addition a significant fraction of particles escape to asymptotic regions. The system eventually settles down to a stable solitonic core state while all the excess kinetic energy is carried away by the escaping particles, which is a phenomenon of gravitational cooling.

1 Introduction

The Schrödinger-Newton system [1, 2, 3] is an interesting example of gravitational non-linear system, which has been studied through numerical analysis. It has a wide range of applications to physics including studies of the measurement problem [4] and the dark matter problem of our Universe [5, 6, 7].

Its numerical studies and the effect of artificial truncation for the treatment of computational domains turn out to be subtle due to the boundary condition imposed at infinity as a significant fraction of particles escape to asymptotic regions for a set of rather generic initial conditions. Thus to be accurate, one has to impose the boundary condition exactly in a numerically reliable manner to avoid the boundary problem arising from the removal of the computational domains. To deal with this issue, a choice adopted in the literature [8] is to use the so-called sponge boundary condition at some large radial position where one imposes a purely absorbing boundary condition. However this involves approximations and it is not clear how the stability of numerical analysis can be maintained with the nonlinear nature of the system. Another alternative is to use a periodic boundary condition but in this case the matter escaping to asymptotic regions are returning to center due to the artificial periodic boundary condition leading to a rather serious finite size effect in some cases.

In this note, we shall follow a different method [9] based on a compact coordinate Y ranged over $[0, 1)$ defined by the relation $Y = \frac{r}{1+r}$ where r is the radial coordinate ranged over $[0, \infty)$. So $r = \infty$ is mapped to $Y = 1$ for instance. Thus at least in principle the boundary condition can be imposed at $Y = 1$ in a straightforward manner. The other part is to use the self-consistent Crank-Nicolson algorithm to see the time evolution of the system starting with a set of initial wave functions which are localized around $Y = 0$. We test our method in a various manner. When the gravity is turned off, we shall compare our result against the corresponding exact solution. In addition, we shall find the relevance of our method with an emphasis on conserved quantities as we shall demonstrate below.

We then study the pattern of gravitational cooling of the system starting with initial condition in which the wavefunction is exponentially decaying in r coordinate. When the total mass is larger than a certain critical value, one finds that a small-sized solitonic core forms as a result of gravitational attraction together with a growing number of excited halo states while a significant fraction of particles escapes to asymptotic regions. Eventually all the excited halo states decay away leaving behind only the stable solitonic core state, which is nothing but the phenomenon of gravitational cooling [10, 11]. In this process, any excess kinetic energy will be released to asymptotic regions with a free streaming flux of particles. In this note, we shall present detailed patterns appearing in this gravitational

relaxation process whose character does not seem to be found elsewhere.

2 Schrödinger Newton Gravity

We shall begin with the Schrödinger-Newton system [1, 2] described by

$$i\hbar\partial_t\psi(\mathbf{x}, t) = -\frac{\hbar^2}{2m}\nabla^2\psi(\mathbf{x}, t) + mV(\mathbf{x}, t)\psi(\mathbf{x}, t) \quad (2.1)$$

$$\nabla^2V(\mathbf{x}, t) = 4\pi GM|\psi|^2(\mathbf{x}, t) \quad (2.2)$$

where the Newtonian potential V satisfies the boundary condition $V \rightarrow 0$ as $r \rightarrow \infty$ and the wavefunction ψ is normalized such that

$$\int d^3\mathbf{x}|\psi|^2 = 1. \quad (2.3)$$

This system consists of many Schrödinger particles of mass m whose total mass is given by M . The wavefunction ψ is describing a Bose-Einstein condensate of the constituent particles. These Schrödinger particles are self-interacting gravitationally, which lead to an integro-nonlinear equation when V is represented by an integration in terms of $|\psi|^2$.

In this system, the total number of particles $N = M/m$ is preserved in time. In addition, the total energy including the gravitation contribution is conserved in time. One may easily show that this conserved energy is given by

$$\mathcal{E} = -\frac{\hbar^2}{2m}\langle\nabla^2\rangle + \frac{m}{2}\langle V\rangle. \quad (2.4)$$

On the other hand, the expectation of the Hamiltonian that is referred as Hamiltonian energy

$$E(t) = \langle H\rangle = -\frac{\hbar^2}{2m}\langle\nabla^2\rangle + m\langle V\rangle \quad (2.5)$$

is time-dependent in general. Below we shall use the conserved total energy and the total probability (2.3) to show the stability and effectiveness of our numerical analysis.

We shall work with dimensionless variables by the following rescaling

$$t \rightarrow \alpha_t t = \frac{\hbar^3}{m^3} \left(\frac{F}{4\pi GM} \right)^2 t \quad (2.6)$$

$$\mathbf{x} \rightarrow \alpha_s \mathbf{x} = \frac{\hbar^2}{m^2} \frac{F}{4\pi GM} \mathbf{x} \quad (2.7)$$

$$\psi \rightarrow \alpha_\psi \psi = \frac{m^3}{\hbar^3} \left(\frac{4\pi GM}{F} \right)^{\frac{3}{2}} \psi \quad (2.8)$$

$$V \rightarrow \alpha_V V = \frac{m^2}{\hbar^2} \left(\frac{4\pi GM}{F} \right)^2 V \quad (2.9)$$

leading to a form suited for the numerical analysis

$$i\partial_t\psi(\mathbf{x}, t) = -\frac{1}{2}\nabla^2\psi(\mathbf{x}, t) + V(\mathbf{x}, t)\psi(\mathbf{x}, t) \quad (2.10)$$

$$\nabla^2V(\mathbf{x}, t) = F|\psi|^2(\mathbf{x}, t) \quad (2.11)$$

which is in terms of the above dimensionless variables. Note that α_ψ and α_V can be given by relations $\alpha_\psi^2\alpha_s^3 = 1$ and $\alpha_V\alpha_t = \frac{\hbar}{m}$ respectively. Below we shall choose $m = 10^{-22}$ eV/ c^2 and F such that

$$F = \frac{M}{10^7 M_\odot} \quad (2.12)$$

with M_\odot denoting the solar mass. This then fixes the time and length scales as

$$\alpha_t \sim 2.36 \times 10^7 \text{ yr} \quad (2.13)$$

$$\alpha_s \sim 0.680 \text{ kpc} \quad (2.14)$$

when $M = 10^7 M_\odot$. With F/M fixed, the scales of our analysis will be fixed. Thus the total mass M of the system will be traded by the parameter F in our numerical analysis.

In this note, we shall mainly be interested in a time evolution of this nonlinear Schrödinger system. One can of course study an eigenvalue problem of the stationary version of the above Schrödinger equation. In the following, we shall restrict our study for the spherically symmetric configuration for the simplicity of our numerical analysis. One is, however, ultimately interested in problems with angular dependence and more complicated problems such as collision of lumps whose nature is truly 3 + 1 dimensional. With the spherical symmetry, the eigenvalue problems can be solved leading to towers of stationary bound states even though the problems involve the nonlinearity. It turns out that all the excited states are unstable under a small perturbation of states and decay to a ground state¹ together with an unbounded stream to asymptotic regions. This surely reflects the nonlinear nature of the problem since in a conventional linear Schrödinger system, this never happens unless there are some other perturbation in its Hamiltonian which derives transitions from one state to another. In our system, the transition occurs without any modification of the Hamiltonian and some significant portions of particles are always ejected to asymptotic regions in this process of relaxation to the ground state.

To see their general features, we shall consider two choices of the initial state

$$\psi_I(r, 0) = \left(\frac{a_I}{\pi}\right)^{\frac{3}{4}} e^{-\frac{a_I}{2}r^2}$$

¹This ground state depends on F together with the final remaining mass for the ground state which is obtained from M by subtracting the mass that is ejected to asymptotic infinity at $t = \infty$.

$$\psi_{II}(r, 0) = \left(\frac{a_{II}^3}{8\pi} \right)^{\frac{1}{2}} e^{-\frac{a_{II}}{2}r} \quad (2.15)$$

which are labeled by I and II respectively. Since the choice of $a_{I,II}$ can be traded with an additional rescaling of F , we shall fix $a_{I,II} = 1$ for the definiteness, which is without loss of generality.

With these initial conditions, we shall numerically study the time evolution of the above equations. Roughly speaking, some part of the initial state will settle down to a ground state while all the remaining will be eventually ejected to asymptotic regions. The final settlement of the ground state is stable under a small state perturbation, which behaves as a kind of soliton². As we shall see, in this process, the innermost core state is rapidly oscillating in general which is surrounded by halos of excited states³ and the oscillation of the core together with halos will eventually decay away either to the ground state or to the asymptotic regions. In this note, we would like to see the details of the time evolution as we change the parameter F .

3 Numerical Setup

Assuming a spherical symmetry, (2.10) and (2.11) become

$$i\partial_t\psi(r, t) = -\frac{1}{2}\frac{1}{r^2}\partial_r(r^2\partial_r\psi(r, t)) + V(r, t)\psi(r, t) \quad (3.1)$$

$$\frac{1}{r^2}\partial_r(r^2\partial_r V(r, t)) = F|\psi|^2(r, t). \quad (3.2)$$

We impose a Neumann boundary condition $\partial_r\psi(0, t) = 0$ at $r = 0$ and a Dirichlet boundary condition $\psi(r, t) = 0$ at $r = \infty$ to have a finite value of the integral $4\pi \int_0^\infty |\psi|^2 r^2 dr$. However this boundary condition at $r = \infty$ is difficult to impose in a numerical analysis of the system. In many cases, people usually impose the Dirichlet condition at $r = R$ with sufficiently large value of R , which introduces unwanted reflection waves at the boundary. To resolve this problem, for instance in [8], a sponge function has been used in finding stationary solutions of (3.1) and (3.2) for removing computational domains. In this work, we employ a different way, since we are interested in outgoing waves in time evolution. We compactify the region $0 < r < \infty$ into a unit interval by introducing a new coordinate variable $Y = \frac{r}{1+r}$. Then there is no issue of reflection waves. In terms of the new

²In some literatures, this state is called as a soliton star.

³These excited states differ from the ones in the above obtained by solving eigenvalue problems since here these states are affected by the presence of the core.

coordinate Y , the radial Laplacian is expressed as

$$\nabla^2 = \frac{1}{r^2} \partial_r (r^2 \partial_r) = \frac{(1-Y)^4}{Y^2} \partial_Y (Y^2 \partial_Y). \quad (3.3)$$

We discretize the spatial interval $0 \leq Y \leq 1$ into N_Y small intervals of the size $\Delta Y = 1/N_Y$. Then we approximate Y by $j\Delta Y$, $j = 0, 1, \dots, N_Y$. The temporal interval is $0 \leq t \leq t_f$. This time interval is discretized N_t times with small intervals of the size $\Delta t = t_f/N_t$. In this way we can approximate the time t by $t = k\Delta t$, $k = 0, 1, 2, \dots, N_t$. The scalar field $\psi(Y, t)$ and the potential function $V(Y, t)$ are replaced with the site variable ψ_j^k and V_j^k . The first derivative and the second derivatives of them are replaced by

$$\partial_Y \psi \rightarrow \frac{\psi_{j+1}^k - \psi_{j-1}^k}{2\Delta Y}, \quad \partial_Y^2 \psi \rightarrow \frac{\psi_{j+1}^k + \psi_{j-1}^k - 2\psi_j^k}{\Delta Y^2} \quad (3.4)$$

for $j = 1, 2, \dots, N_Y - 1$. On the other hand for $j = 0$, this replacement becomes singular. Instead, we use the relation

$$\nabla^2 \psi|_{r=0} = 3\partial_r^2 \psi|_{r=0} = 3[(1-Y)^4 \partial_Y^2 - 2(1-Y)^3 \partial_Y] \psi|_{Y=0} \quad (3.5)$$

assuming the spherical symmetry. Its discretized version reads

$$\nabla^2 \psi|_{r=0} \rightarrow 3 \left(\frac{\psi_{-1} + \psi_1 - 2\psi_0}{\Delta Y^2} - 4 \frac{\psi_1 - \psi_{-1}}{\Delta Y} \right) = 6 \frac{\psi_1 - \psi_0}{\Delta Y^2} \quad (3.6)$$

where the Neumann boundary condition is implemented by setting $\psi_{-1} = \psi_1$ to get the last equality.

In consideration of time evolution, we use Crank-Nicolson method for stability of the system. With the discrete time, (3.1) becomes

$$i \frac{\psi^{k+1} - \psi^k}{\Delta t} = \frac{1}{2} \left\{ \left(-\frac{1}{2} \nabla^2 \psi^{k+1} + V^{k+1} \psi^{k+1} \right) + \left(-\frac{1}{2} \nabla^2 \psi^k + V^k \psi^k \right) \right\}. \quad (3.7)$$

(In this equation we have suppressed spatial indices for a clear presentation of our method for time evolution.) Note that we take an average of two values at different time-indices k and $k+1$. Supposing that we know the values of the wavefunction up to the time index k , (3.7) implicitly determines ψ^{k+1} at next time. To find an explicit form we arrange this equation

$$\left[1 - \frac{\Delta t}{2i} \left(-\frac{1}{2} \nabla^2 + V^{k+1} \right) \right] \psi^{k+1} = \left[1 + \frac{\Delta t}{2i} \left(-\frac{1}{2} \nabla^2 + V^k \right) \right] \psi^k. \quad (3.8)$$

In the case of ordinary linear Schrödinger equation, the potential V is time independent and then we might directly obtain ψ^{k+1} by inverting $\left[1 - \frac{\Delta t}{2i} \left(-\frac{1}{2} \nabla^2 + V \right) \right]$. But in our case,

the potential V^k is a solution of (3.3) depending on ψ^k and thus V^{k+1} involves unknown function ψ^{k+1} . So we determine ψ^{k+1} in an iterative procedure. Let us approximate V^{k+1} by V^k at initial stage, then we may obtain an approximate value of ψ^{k+1} by inverting $[1 - \frac{\Delta t}{2i}(-\frac{1}{2}\nabla^2 + V^k)]$. With this ψ^{k+1} , we solve the second equation (3.2) to find a improved value of V^{k+1} . In the second stage, we may obtain an improved value for ψ^{k+1} by inverting the left hand side of (3.8) with the improved V^{k+1} obtained in the previous step. By repeating this procedure, we can find very accurate value for ψ^{k+1} .

Below we shall be mainly interested in the probability density distribution in Y space given by

$$\rho_Y(Y, t) = 4\pi \frac{Y^2}{(1 - Y)^4} |\psi(Y, t)|^2. \quad (3.9)$$

The time dependent flow of the probability density will give us a detailed information on the dynamics of Schrödinger-Newton system. Further we shall be interested in a rotation curve defined by the relation

$$v(r, t) = \sqrt{\frac{G\mathcal{M}(r, t)}{r}} \quad (3.10)$$

where $\mathcal{M}(r, t)$ is defined by the integrated mass within the radius r that is given by

$$\mathcal{M}(r, t) = 4\pi M \int_0^r dr' r'^2 |\psi(r', t)|^2. \quad (3.11)$$

4 Results

In this section we present various types of benchmarks of the Crank-Nicolson method, which verify that the self-consistent optimization scheme we employ performs efficiently for a wide range of discretization parameters. We also demonstrate that the use of the self-consistent technique has potential advantages such as favorable scaling in reducing the step sizes in both time and space, and the ease with which can be applied to more complicated nonlinear equations.

Figure 1 summarizes the performance of the self-consistent Crank-Nicolson method for a non-interacting Schrödinger-Newton equation as a function of time and the step sizes in both space and time. At $F = 0$ the model is analytically tractable if the initial wavefunction is of the form of the first type. In Figures 1(a) and (c) ((b) and (d)), we show how the mean absolute error of the real (imaginary) part in the wavefunction, defined as $\Delta\psi = \sum_i^{N_Y} |\psi_i^{CN} - \psi_i^{exact}|$, changes as a function of time and the step size

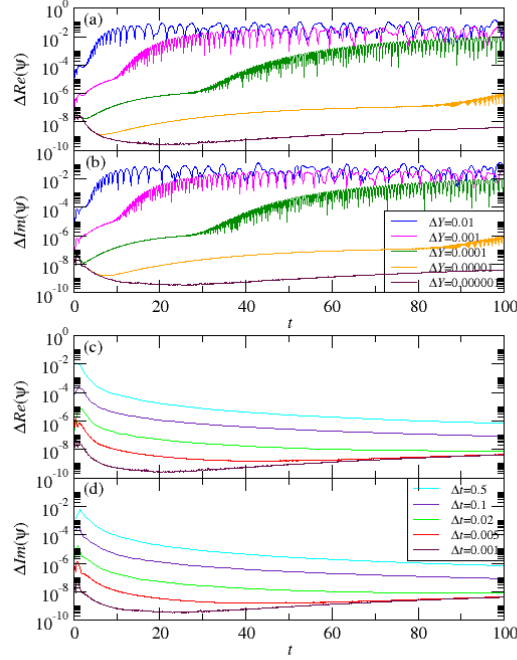


Figure 1: Mean absolute error in the wavefunction using the Crank-Nicolson method as a function of time (see text), for (a) $Re(\psi_I)$, $\Delta t=10^{-3}$, (b) $Im(\psi_I)$, $\Delta t=10^{-3}$, (c) $Re(\psi_I)$, $\Delta Y=10^{-6}$, and (d) $Im(\psi_I)$, $\Delta Y=10^{-6}$. The initial wavefunction we use is of the form $\psi_I(r, 0) = \pi^{-3/4} e^{-\frac{1}{2}r^2}$, and $F=0$.

in time Δt (space ΔY). As can be seen in Figures 1(a) and (b), for large spatial step sizes we find an oscillatory behavior in the error corresponding to numerical instability, which characterizes the deterministic nature of the numerical algorithm as well as the exact treatment of the boundary condition at infinity. Importantly, the decrease of the step size in space would alleviate the problem of numerical stability on finite difference discretization. As shown in Figures 1(a) and (b), the error of our method decreases as a power law in step sizes.

The complete energy results, summarized in Figures 2 and 3 are notable. In all cases, while the calculated Hamiltonian energy corresponding to the expectation of the Hamiltonian $\langle H \rangle$ does not preserve in time, the total conserved energy \mathcal{E} to be gained from the gravitational interaction is independent of time as was mentioned previously. Figure 2(a) (3(a)) shows the total energy in the wavefunction of the first (second) type as a function of time for a region $44 \leq F \leq 52$ ($15 \leq F \leq 19$), where an almost stationary state occurs for F nearly at 48 (17). The amplitude of energies grows with increasing the

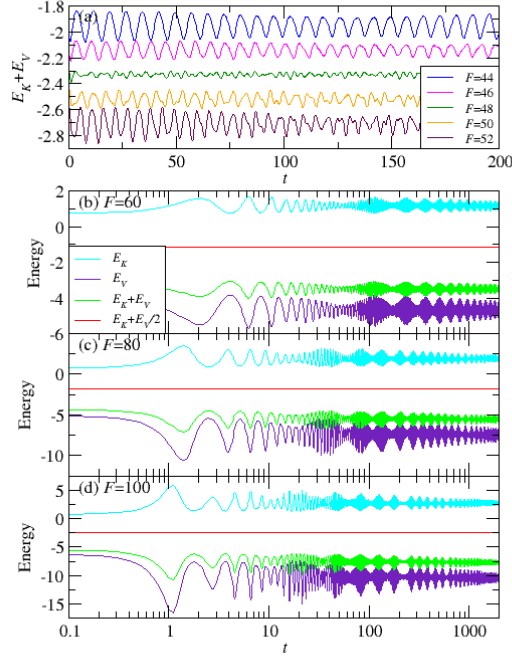


Figure 2: (a) $E_K + E_V$ for the initial wavefunction of the form $\psi_I(r, 0) = e^{-r^2/2}/\pi^{3/4}$ as a function of time and the parameter F . A stationary state occurs at $F = 48$. The energy as a function of time for (b) $F = 60$, (c) $F = 80$, and (d) $F = 100$. In all panels, E_K denotes the kinetic energy, E_V the potential energy, $E_K + E_V$ the Hamiltonian energy, and $E_K + E_V/2$ the conserved energy. Here $\Delta t = 10^{-3}$ and $\Delta Y = 10^{-6}$.

magnitude of F , and decreases as time is increased. Our numerical results demonstrate that the period strongly depends on the magnitude of F as well as initially excited states settle into stable ground state together with the asymptotic streamline of particles.

Let us now present our main results of numerical analysis. Here in this presentation, we shall use the initial condition ψ_{II} given in (2.15). Our primary focus is the time development of the probability density $\rho_Y(Y, t)$ in the Y space. Let us first illustrate its general trends as the parameter F (or the total mass M) changes.

If F is small enough, there is in general a negligible gravitational attraction compared to the kinetic part of energy. Ignoring the potential contribution, the system follows the dynamics of free Schrödinger system where eventually all the probability will spread out completely as t goes to infinity. This feature is clearly seen in the first row of Figure 4, which is for $F = 5$. There is no small-sized left-over core state while most of the probability spreads out to asymptotic regions.

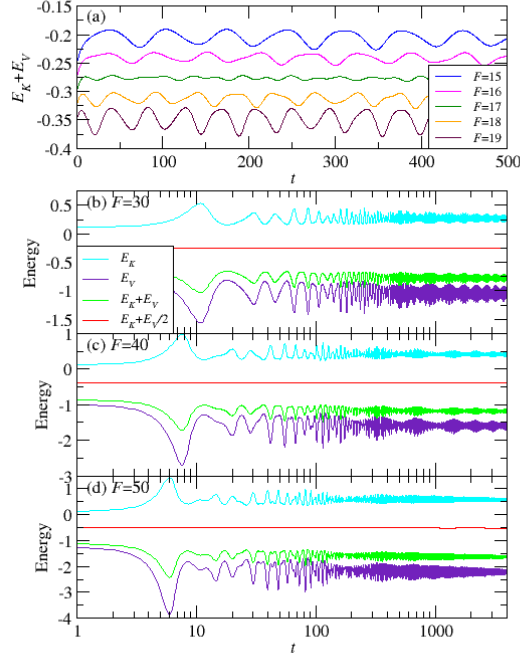


Figure 3: (a) $E_K + E_V$ for the initial wavefunction of the form $\psi_{II}(r, 0) = e^{-r/2}/\sqrt{8\pi}$ as a function of time and the parameter F . A stationary state occurs at $F = 17$. The energy as a function of time for (b) $F = 30$, (c) $F = 40$, and (d) $F = 50$. In all panels, E_K denotes the kinetic energy, E_V the potential energy, $E_K + E_V$ the Hamiltonian energy, and $E_K + E_V/2$ the conserved energy. Here $\Delta t = 10^{-3}$ and $\Delta Y = 10^{-6}$.

When F is around $F_0 \sim 17$, there is a change of the above trend as mentioned previously. Our initial configuration ψ_{II} is rather close to that of the stable solitonic core state which is the lowest energy eigenstate of the corresponding Schrödinger-Newton system. This stable soliton core state is the remnant state after completion of the gravitational cooling. F_0 in the above is defined by the relation $\langle r \rangle_{\psi_{II}} = \langle r \rangle_{\text{soliton-core}}(F_0)$ where one equates the expectation value of r with the initial state ψ_{II} with the expectation value of r of the solitonic core state as a function of F . When $F = F_0$, one finds that the escape probability is minimized and the state remains almost stationary as was shown the second row of Figure 4.

When F is larger than F_0 , the gravitational attraction of the initial configuration is big enough to form a small-sized solitonic core state as one can see in Figures 4, and 5. Further significant fraction of particles are escaping to asymptotic regions, which is reflecting basically the phenomenon of gravitational cooling. In this regime, we depict a little

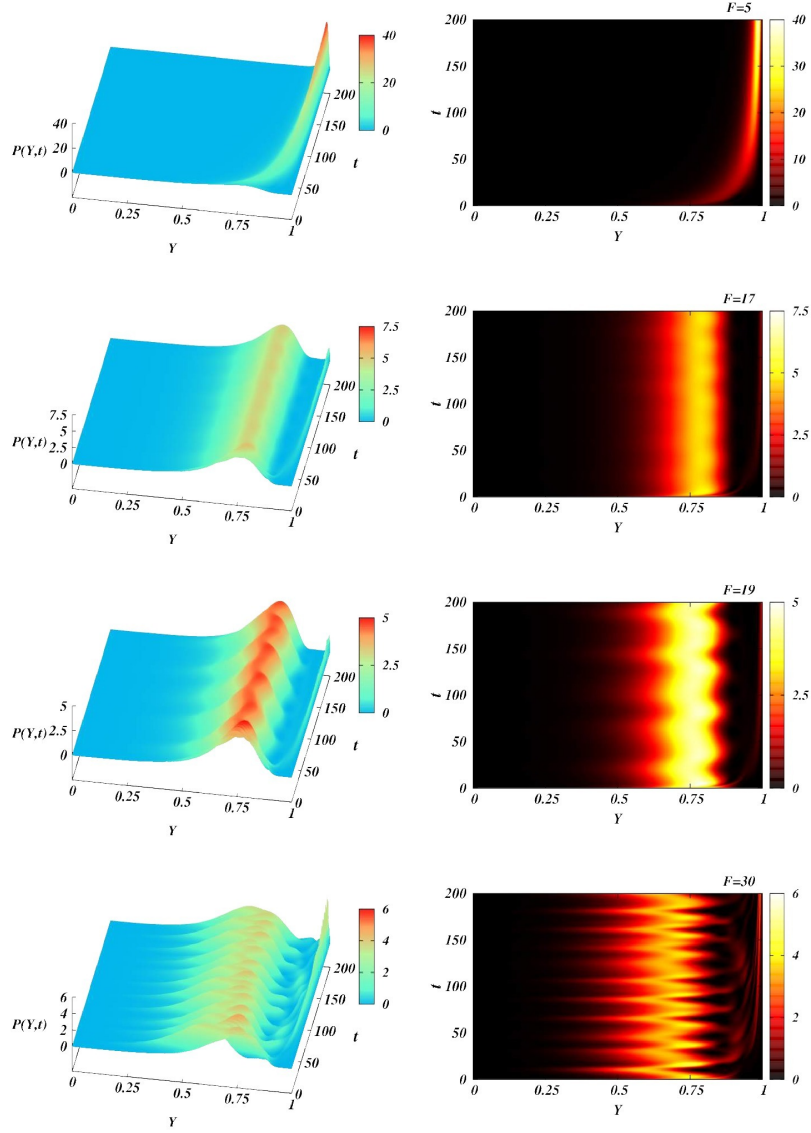


Figure 4: The probability densities in Y space are depicted for the values of $F = 5, 17, 19,$ and 30 (from the top to the bottom row) with the initial condition ψ_{II} .

detailed feature in Figure 5 for $F = 50, 100, 150,$ and 200 up to $t = 200$. One can see that a small-sized solitonic core is forming rapidly whose average location in Y coordinate gets smaller as F becomes larger and larger. This is because the effective gravitational attractions become larger as F gets larger. Interestingly, this core is rapidly oscillating with multiple number of frequencies reflecting nonlinear nature of our Schrödinger-Newton system. One sees that part of rapid oscillation around peak radial position is escaping to larger distance forming the number of excited states. These excited states are unstable

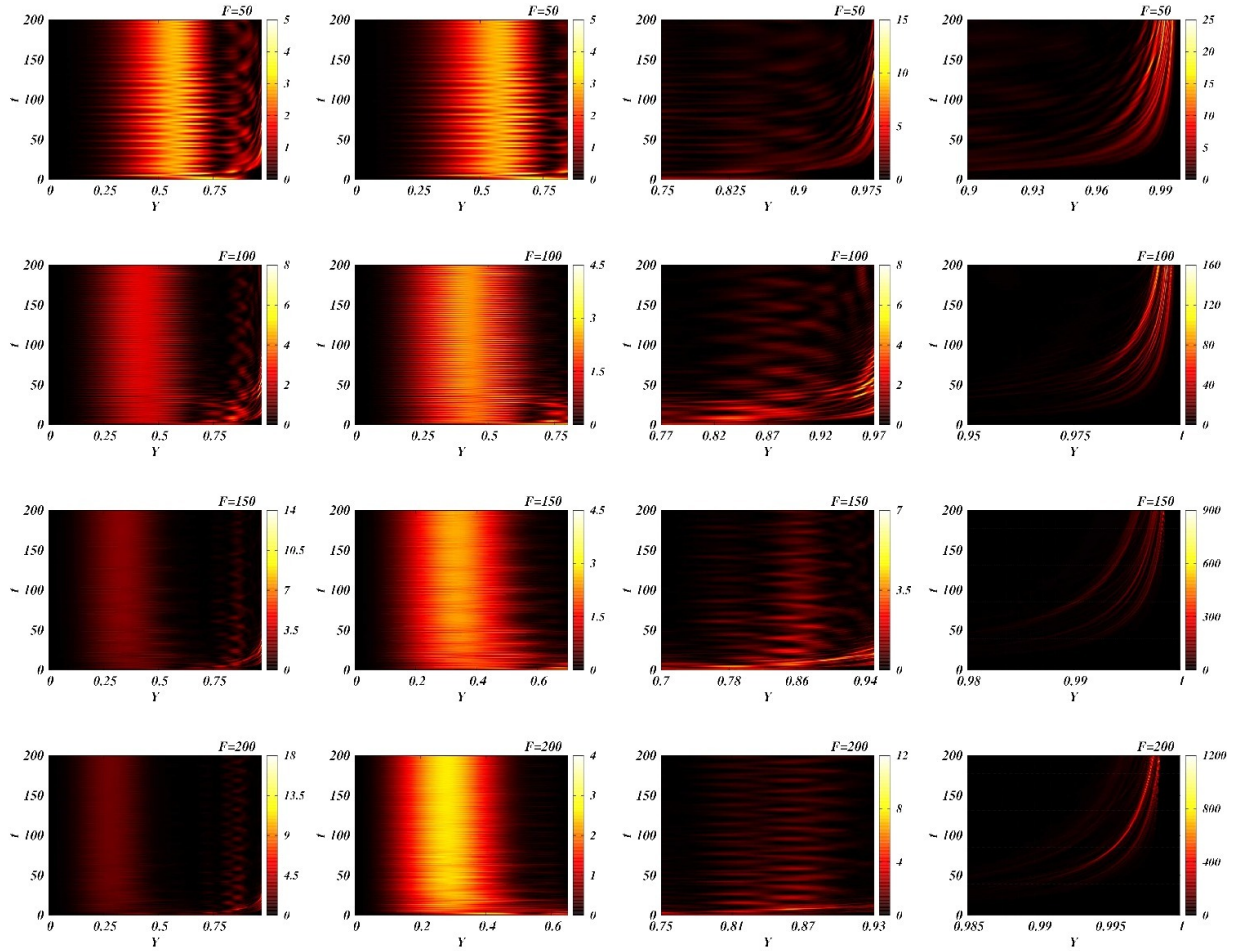


Figure 5: The probability densities in Y space are depicted for the values of $F = 50, 100, 150,$ and 200 from the top line to the bottom with the initial condition ψ_{II} . The first column is for the full region of $Y \in [0, 1)$ and the second and the third are zooming the solitonic core and excited states respectively. One can see the escaping streaming of probability current to the asymptotic region in the fourth column.

and decay completely escaping to infinity eventually. Such feature is depicted in Figure 5. In the figures in the first column of Figure 5, we draw $\rho_Y(Y, t)$ for the entire range of Y . The figures in the second/third column illustrate solitonic cores/excited halo states. The figures in the fourth column are for the streamlined flow of probability escaping to asymptotic regions. In the left panel of Figure 7, we also show the 3D diagram of $\rho_Y(Y, t)$ for $F = 200$ and one can see the feature of gravitational cooling in a rather clear manner.

Figure 6(a) shows the escape probability $P(r > 24)$ as a function of time which is an integrated probability of finding particles in the region beyond $r = 24$. We choose

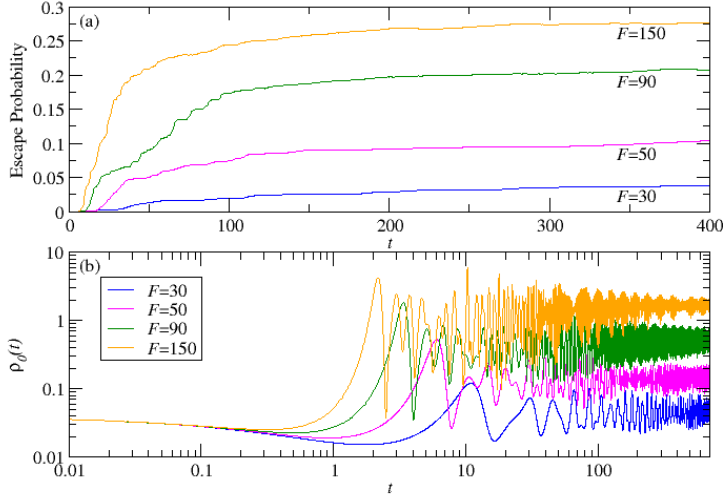


Figure 6: We present the escaping probabilities in the region beyond $r = 24$ (or $Y = 0.96$) on the left and the values of $\rho_0(t) = |\psi(0, t)|^2$ at the origin as functions of time, for the cases $F = 30, 50, 90,$ and 150 .

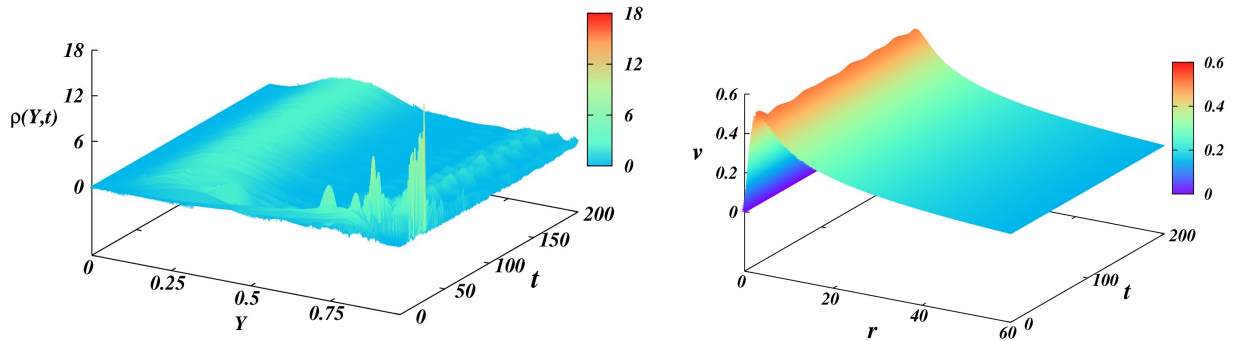


Figure 7: On the left the probability density in Y space is depicted as 3D diagram for $F = 200$ with the initial condition ψ_{II} . One can see the escaping streaming of probability current to the asymptotic region. On the right, we draw the rotation curve v for $F = 17$.

$F = 30, 50, 90$ and 150 . There is always an initial time delay since the initial flow of particles needs time to reach $r = 24$. As seen in Figure 6(a), the maximum time delay for

$F = 150$ is approximately 10. After the delay, there is rather a stiff growth of probability in time which saturates to a certain value eventually. The full escape probability is around 0.38 when $F = 200$ for instance. As shown in Figure 6(a), the escape probability is strongly enhanced as F increases.

Figure 6(b) also shows the central density $\rho_0(t) = |\psi(0, t)|^2$ for $F = 30, 50, 90,$ and 150 , hence, one finds they are oscillating rapidly as found in the corresponding solitonic cores and settle down to certain values eventually as the gravitational cooling progresses.

Figure 7 emphasizes the peculiar features of the system that have been found in our numerical calculations. The left panel of Figure 7 shows the escaping streaming of probability current to the asymptotic region in the presence of strong gravity for $F = 200$ ($\gg F_0$), confirming that gravity interactions strongly affect the characteristic of gravitational cooling. In the right panel of Figure 7, we further show the rotation curve v as functions of t and r which again displays the stationary nature of $F = 17$ configuration as the probability in Figure 3.

5 Discussions

In this note, we numerically study time evolution of the spherically symmetric Schrödinger-Newton system using the self-consistent Crank-Nicolson approach. Compactification of radial coordinate enables us to investigate gravitational cooling patterns in a reliable way. It is shown that the numerical errors are successfully controlled. Our simulation clearly shows that a small-sized solitonic core forms accompanied with number of excited halo states and a large fraction of particles escape to asymptotic regions. Besides these common features, it also shows how the patterns of these gravitational coolings depend on the values of total mass.

Even if our work is limited to spherically symmetric cases in this work, it should be interesting to study possible angular structures of Schrödinger-Newton system with or without axial symmetry. This will be our next work. Another interesting direction of research is numerical simulation of very large structures in super-galactic scale. Recent simulations assumed cold dark matter. It is very intriguing to see the results of simulations involving self gravitating Schrödinger field instead of cold dark matter [7] in a rather detailed manner.

Acknowledgement

D.B. was supported in part by 2018 Research Fund of University of Seoul.

References

- [1] L. Diósi, “Gravitation and quantum mechanical localization of macro objects,” *Phys. Lett. A* **105**, 199 (1984) [arXiv:1412.0201 [quant-ph]].
- [2] I. M. Moroz, R. Penrose and P. Tod, “Spherically symmetric solutions of the Schrodinger-Newton equations,” *Class. Quant. Grav.* **15**, 2733 (1998).
- [3] M. Bahrami, A. Großardt, S. Donadi and A. Bassi, “The Schroedinger-Newton equation and its foundations,” *New J. Phys.* **16**, no. 11, 115007 (2014) [arXiv:1407.4370 [quant-ph]].
- [4] J. R. van Meter, “Schrodinger-Newton collapse of the wave function,” *Class. Quant. Grav.* **28**, 215013 (2011) [arXiv:1105.1579 [quant-ph]].
- [5] L. Hui, J. P. Ostriker, S. Tremaine and E. Witten, “Ultralight scalars as cosmological dark matter,” *Phys. Rev. D* **95**, no. 4, 043541 (2017) [arXiv:1610.08297 [astro-ph.CO]].
- [6] J. W. Lee, “Brief History of Ultra-light Scalar Dark Matter Models,” *EPJ Web Conf.* **168**, 06005 (2018) [arXiv:1704.05057 [astro-ph.CO]].
- [7] H. Y. Schive, T. Chiueh and T. Broadhurst, “Cosmic Structure as the Quantum Interference of a Coherent Dark Wave,” *Nature Phys.* **10**, 496 (2014) [arXiv:1406.6586 [astro-ph.GA]].
- [8] P. Salzman: “Investigation of the Time Dependent Schrödinger- Newton Equation”, Ph.D. thesis, Univ. of California at Davis, 2005.
- [9] D. Bak, M. Gutperle and R. A. Janik, “Janus Black Holes,” *JHEP* **1110**, 056 (2011) [arXiv:1109.2736 [hep-th]]. D. Bak, C. Kim, K. K. Kim, H. Min and J. P. Song, “Geometric Monte Carlo and Black Janus Geometries,” *Phys. Lett. B* **767**, 341 (2017) [arXiv:1611.10255 [hep-th]].
- [10] F. S. Guzman and L. A. Urena-Lopez, “Evolution of the Schrodinger-Newton system for a selfgravitating scalar field,” *Phys. Rev. D* **69**, 124033 (2004) [gr-qc/0404014].
- [11] F. S. Guzman and L. A. Urena-Lopez, “Gravitational cooling of self-gravitating Bose-Condensates,” *Astrophys. J.* **645**, 814 (2006) [astro-ph/0603613].